Running Head: Lugworm irrigation and nitrogen cycling

A modeling study of lugworm irrigation behavior effects on sediment nitrogen cycling

TM Dornhoffer[1], GG Waldbusser[2] and C Meile[1*]

[1]Department of Marine Sciences, The University of Georgia, Athens GA 30602
[2]College of Earth, Ocean, and Atmospheric Sciences, Oregon State University, Corvallis OR 97331
[*]Corresponding author: cmeile@uga.edu

Abstract

Benthic infauna in marine sediments have well-documented effects on biogeochemical cycling, from individual to ecosystem scales, including stimulation of nitrification and nitrogen removal via denitrification. However, the effects of burrowing depth and irrigation patterns on nitrogen cycling have not been as well described. Here we examine the effects of lugworm behavior on sediment nitrogen cycling using a reaction-transport model parameterized with literature and laboratory data. Feeding pocket depth and pumping characteristics (flow rate and pattern) were varied, and rates of nitrification, denitrification, and benthic exchange fluxes were computed. As expected, more intense burrow irrigation stimulates denitrification and coupled nitrification-denitrification. At high pumping rates and low sediment oxygen consumption rates (~10^{-6} mol m^{-3} s^{-1}), simulation results show a decrease in rates of nitrification and denitrification with decreasing burrow depth due to incomplete consumption of injected oxidants. Model results also suggest that discontinuous irrigation leads to temporal variability in sediment nitrogen cycling, but that the time-averaged rates do not depend on the irrigation pattern. We identify 1) the poorly constrained chemical composition of lumen fluid injected into sediments and 2) the response of microbial activity/distribution to oscillating redox conditions as critical knowledge gaps affecting estimates of sediment N removal.

Keywords: Arenicolid, bioirrigation, benthic-pelagic coupling, denitrification

Introduction

Nitrogen is an essential nutrient in marine systems that can control productivity and – in excess – lead to coastal eutrophication and hypoxia (Diaz & Rosenberg 2008, Pearl & Piehler 2008, Canfield et al. 2010). Eutrophication and the subsequent advent of coastal ocean hypoxia can have severe negative effects on the marine community, with pronounced impacts on benthic macrofaunal diversity and composition (Levin et al. 2009, Zhang et al. 2010) as well as individual behavior (Riedel et al. 2014). These impacts in turn compromise the ecosystem services that the benthos provides, including organic matter recycling and nitrogen removal (Cloern 2001, Diaz & Rosenberg 2008). The loss of these essential ecosystem functions can have wide-ranging ecological consequences, even exacerbating the hypoxia problem by enhancing nitrogen recycling rather than removal (Kemp et al. 2005).

One of the most significant nitrogen sinks in coastal environments is denitrification, whereby nitrate is reduced to molecular nitrogen gas and thus becomes biologically unavailable. Denitrification is inhibited by oxygen, and is typically confined to sediments where the aerobic degradation of organic material exhausts dissolved oxygen. Nitrogen is supplied to the sediment both via transport from the overlying water, and from organic matter degradation, which supplies ammonium that undergoes nitrification to nitrate and subsequently can be consumed through denitrification by coupled nitrification-denitrification (Seitzinger 1988, Galloway et al. 2004). Efficiently coupled nitrification-denitrification is reliant on the close proximity of oxic and anoxic zones in sediments, and so the fate of nitrogen is affected heavily by sediment oxygen distribution (Kristensen et al. 1987), which in many coastal sediments is substantially influenced by macrofauna (e.g. Volkenborn et al. 2012).

Benthic infauna can significantly enhance rates of elemental cycling (Henriksen et al. 1983, Huettel 1990, Aller & Aller 1998, Banta et al. 1999) and alter the distribution and cycling of nitrogen through a variety of means. At the most basic level, the formation of burrow structures enhances benthic-pelagic coupling by creating a larger surface area for diffusive exchange (Aller 2001). Burrowing also accelerates the dispersion of solid particles - including organic matter - in the sediment (Fornes et al. 1999, Berg et al. 2001), and in large-scale *Arenicola* exclusion experiments, Volkenborn et al. (2007a) observed significant changes to both sediment structure and composition as a result of the presence or absence of adult arenicolid polychaetes. These changes directly affect the permeability of sediments, enhancing the transport of solutes caused by advective flow. At the burrow scale, irrigation in permeable sediments results in the injection of oxic seawater into otherwise reducing sediment (D'Andrea et al. 2002, Waldbusser & Marinelli 2006, Volkenborn et al. 2010), which powers a cascade of redox reactions. However, although the individual time-averaged effects of bioirrigation have been extensively studied and modeled, ecosystem function of complex communities (as measured by e.g. remineralization rates) is often poorly estimated by summation of the known individual effects (Waldbusser et al. 2004).

One of the key challenges in predicting the function of complex ecosystems is the delineation of relationships between community characteristics and ecosystem function. Several studies have documented statistically significant relationships between ecosystem function and biogeochemical settings, macrofaunal diversity or density (Emmerson et al. 2001, Marinelli et al. 2003, Waldbusser et al. 2004, Norling et al. 2007, D'Andrea et al. 2009, Michaud et al. 2009, Waldbusser & Marinelli 2009), but these correlations tend to be unable to entirely predict ecosystem function (Waldbusser et al. 2004, Norling et al. 2007). This may be due in part to variations in organism behavior affecting burrow spacing - which can alter benthic oxygen fluxes (Dornhoffer et al. 2012) and rates of nitrification and denitrification (Gilbert et al. 2003) - or burrowing depth, which could potentially impact oxygen distribution (Michaud et al. 2009) and fluid residence times (e.g. Santos et al. 2012).

Our limited knowledge of the importance of variations in organism behavior is related at least in part to the scarcity of measured reaction rates at the spatial and temporal resolution necessary to capture redox oscillations in the vicinity of burrows (Marinelli & Boudreau 1996, Volkenborn et al. 2010, Volkenborn et al. 2012). Numerical reaction transport models of multiple chemical species can help fill this gap by providing high-resolution calculated concentration fields and reaction rates. In this paper we present a modeling study parameterized with laboratory and literature data to determine the effects of a common lugworm, *Abarenicola pacifica,* on sediment nitrogen cycling. Lugworms (Family Arenicolidae) are a group of polychaete annelid commonly found in sandy coastal areas across a worldwide distribution. These head-down deposit feeders are considered ecosystem engineers because their presence and actions have a formative effect on their ecosystems, influencing the physical, chemical, and ecological makeup of their communities

(Volkenborn et al. 2007a, Volkenborn 2007b). Specifically, we investigate 1) to what extent increasing burrow irrigation rates increase rates of nitrogen cycling, 2) the extent to which changes in burrow depth alter the rates of nitrification and denitrification, and 3) the implications of different irrigation patterns, particularly the importance of continuous vs. discontinuous irrigation. We use the model results to yield insight into the major controls of benthic nitrogen cycling and highlight important areas for future investigation.

Methods

Microcosm Methods

In order to determine the impacts *Abarenicola pacifica* has on solute exchange, five microcosms (15 cm radius by 45 cm deep) were established and filled with homogenized sediments to a depth of 30 cm, which was allowed to settle for 2 weeks. Sediment and organisms were collected from tide-flats in Yaquina Bay, OR, USA, and microcosms were maintained in a flow-through seawater tank at the Hatfield Marine Science Center, Newport, OR. Salinity and temperature of incubation tanks were subjected to variations in source water from Yaquina Bay and were 28-30 and 8-12^{o}C, respectively. After 2 months acclimation, fluxes of oxygen, ammonium and nitrate were measured in closed incubations with magnetic stirrers attached to a fishing wire inside the microcosm to agitate overlying water without creating radial pressure gradients. Incubations were run on December 20 and 30, 2009, and January 6 and 20, 2010. During each incubation, overlying water samples (~5 ml) were taken every 1-1.5 hours until either oxygen levels dropped to 50% of the starting value or 4 samples were taken. In all cases, at least 3 data points were collected, and the change in overlying water concentration was used to compute benthic fluxes. Oxygen samples were measured with an oxygen optode (PSt1, PreSens), and nutrient samples were 0.2 μm filtered then frozen in sterile sample vials. Nutrient samples were analyzed colorimetrically following the protocols of Waldbusser & Marinelli (2006).

Sediment reaction rates were determined at the termination of the microscosm study (Feb 1, 2010). Approximately 2 ml sediment samples were collected at depth intervals of 0-2, 2-5, 5-10, 10-15, 15-20, 20-25 cm and incubated as a slurry with 2 ml of filtered seawater on a shaker table. Oxygen concentrations were measured every 2-3 hours and oxygen consumption rates were computed from the linear decrease in dissolved oxygen over time. O_2 consumption rates were then used to estimate the rate constant for organic matter mineralization (k_{DOM}, see below).

Model Description

A cylindrical model domain with a radius of 10 cm was established, containing a single lugworm injection pocket located on the central symmetry axis. These dimensions were chosen to represent typical organism densities (Volkenborn et al. 2007b). The domain encompasses 2 cm of water overlying 20 cm sediment with a constant porosity of 0.6, and a constant permeability (k = 1 x 10^{-12} m^2, after Volkenborn et al. 2010) except for a feeding column of radius 0.025 m located above the spherical injection pocket (Huettel 1990, Retraubun et al. 1996), with a permeability an order of magnitude greater than the surrounding sediment (k = 1 x 10^{-11} m^2) as a first-order approximation. The porosity used is slightly higher than the laboratory-measured porosity, which has negligible impacts on volume-integrated reaction rates. The tailshaft was not explicitly modeled because its presence has been shown to have negligible effects on sediment flow fields (Meysman et al. 2006).

In conjunction with an incompressibility condition (Eq. 1c), fluid flow was simulated using the Navier-Stokes equation in the overlying water (Eq. 1a). Flow in the sediment was modeled using the Stokes-Brinkman equation (Eq. 1b), which neglects the inertial term in the porous medium but accounts for the exchange of stress between the fluid and the sediment matrix (Bars & Worster 2006):

$$\rho\frac{\partial u}{\partial t} + \rho(u\cdot\nabla)u = \nabla\cdot\left[-p\mathrm{I} + \mu_{eff}(\nabla u + (\nabla u)^T)\right] \quad (1a)$$

$$\frac{\rho}{\emptyset}\frac{\partial u}{\partial t} = \nabla\cdot\left[-p\mathrm{I} + \frac{\mu}{\phi}(\nabla u + (\nabla u)^T) - \frac{2\mu}{3\phi}(\nabla\cdot u)\mathrm{I}\right] - \left(\frac{\mu}{k}\right)u \quad (1b)$$

$$\rho\nabla\cdot u = 0 \quad (1c)$$

where ρ is the fluid density, u is the flow velocity (in the sediment, eq. 1b, this is the Darcy velocity), p is the pressure, I is the identity tensor, k is the permeability, ϕ is the porosity, μ is the dynamic viscosity of 0.001 Pa-s, and μ_{eff} is the depth-dependent effective dynamic viscosity term in the overlying water composed of the dynamic viscosity plus the eddy viscosity *E(z),* as determined by the Reichardt equation (Eq. 2), times the fluid density:

$$E(z) = \kappa z u_*[1 - \left(11/(\frac{\rho z u_*}{\mu})\right)\tanh\left(\frac{\rho z u_*}{11\mu}\right)] \quad (2)$$

where κ is the Karman constant of 0.4, z is the height above the sediment-water interface in meters and u_* is the shear velocity, set to 0.1 cm s^{-1} (Boudreau 2001). The bottom and side of the cylindrical domain were set as no flow boundaries, while at the upper boundary, atmospheric pressure was imposed, allowing for the flow of water. The boundaries of the feeding pocket served as the porewater injection site, with a pumping rate imposed (as an input velocity for a given feeding pocket size). In simulations with discontinuous irrigation, a 5-minute period of pumping at a constant rate followed by 5 minutes of resting was imposed, following the general pumping pattern reported by Volkenborn et al. (2010). In the case of continuous irrigation, the input velocity was halved relative to that in the corresponding discontinuously irrigated model, so that the time-integrated flow rate was the same.

The distributions of nine dissolved chemicals were computed as

$$\phi \frac{\partial C}{\partial t} = \nabla \cdot (D\phi \nabla C) - \nabla \cdot (uC) + R \qquad (3)$$

where D is the effective diffusion coefficient, C is the concentration, and R is the net reaction rate, reflecting the reactions listed in Table 1 within the sediment and set to 0 in the overlying water. In the sediment, the effective diffusion coefficient for solutes reflected molecular diffusion corrected for tortuosity ($D = D_{mol}/(1 - \ln(\phi^2))$), while in the overlying water, the effective diffusion coefficient also accounted for eddy diffusion, $D = D_{mol} + E(z)$, using the Reichardt equation (Eq. 2) in order to simulate well-mixed overlying water above the diffusive boundary layer. This approach was necessary because advective flow induced by infauna can influence solute concentrations at the SWI (Volkenborn et al. 2010), and therefore the concentrations must be imposed sufficiently high above the SWI to avoid interference with this effect. A reaction network describing the breakdown of organic matter was implemented, consisting of 9 reactions (Table 1), following the general approach of Van Cappellen & Wang (1996) and Porubsky et al. (2011). Nitrate is removed via denitrification; not included are dissimilatory nitrate reduction to ammonium (DNRA) and anaerobic ammonium oxidation (anammox). DNRA has been shown to be responsible for a large portion of nitrate reduction (Christensen et al. 2000, An et al. 2002, Gardner et al. 2006, Lam et al. 2011), but typically is most prevalent under sulfidic conditions (Koop-Jakobsen et al. 2010) that are not present in the irrigated scenarios considered here. Anammox tends to be important under anoxic conditions with relatively low sediment organic material loading (Engstrom et al. 2005), but in shallow water coastal environments with plentiful organic matter such as those modeled here, it generally accounts for a small percentage of total N_2 production (Thamdrup & Dalsgaard 2002, Dalsgaard et al. 2005, Engstrom et al. 2005, Thamdrup 2012). Finally, assimilation of nitrogen into new biomass could account for a significant portion of remineralized nitrogen sequestration (Sundbaeck et al. 2004). However, this amount is poorly constrained, and so was not included in the model formulation.

Rate constants for sediment reactions and their sources are presented in Table 2. Most were obtained from the literature, though the rate constant of the organic matter degradation k_{DOM} was based on incubation experiments in which the consumption of O_2 was observed over time. Using an assumed reactive dissolved organic carbon (DOM) porewater concentration of 115 μM, in line with measured total porewater DOC (Alperin et al. 1999), the average oxygen consumption rate (R) measured in slurries was used to approximate k_{DOM}, such that k_{DOM} = R/DOM and k_{POM}

= R/POM (POM determined from loss on ignition of sediment). This assumes that DOM consumption and production from POM are balanced during the slurry incubation. Although we cannot entirely rule out oxygen consumption by reoxidation of metabolites, we assume that oxygen consumption directly reflects OM degradation because lugworm irrigation leads to depletion of reduced metabolites (e.g. Volkenborn et al. 2007a).

For solutes, domain sides and bottom were impermeable, and a fixed concentration was imposed at the top and at the injection pocket based on laboratory data; reduced substances were assumed to have a concentration of 0 at the upper boundary and in the burrow lumen. The model was implemented in COMSOL Multiphysics 4.4. The 2D axisymmetric domain was discretized into approximately 50,000 finite elements. Models were run to steady state using generalized-alpha time-stepping (Chung et al. 1993); in the case of discontinuous models a maximum time step of 50 s was imposed in order to properly capture temporal variability over a pumping cycle.

To document the effects of burrow depth, feeding pockets were established in the models at 5, 10 or 15 cm depth. Additionally, in order to examine the importance of environmental context, the rate constants of organic matter mineralization and nitrification, and the concentrations of NO_3 and DOM in the injected porewater were varied.

Results

Microcosm

Lugworm irrigation and nitrogen cycling

Ventilation of burrows by *A. pacifica* led to the formation of deep oxic pockets in otherwise anoxic sediments. The typical O_2 penetration depth (as indicated by the redox color discontinuity) was 1 – 2 mm below the sediment-water interface, except around the feeding pocket, where sediments were oxidized more uniformly in the microcosm around the feeding pocket. O_2 consumption rates measured in slurry incubations of microcosm sediment were 1.17 ± 0.49 (1 SD) μmol m^{-3} s^{-1}, giving values of 1.017 x 10^{-5} s^{-1} and 7.9 x 10^{-9} s^{-1} for k_{DOM} and k_{POM}, respectively (using a POM concentration of 150 mol m^{-3} based on loss on ignition). Nitrate and oxygen fluxes measured in the microcosm experiments were on the order of 1 and 50 mmol m^{-2} d^{-1}, respectively (Table 3).

Model simulations

Pressure imposed by lugworm irrigation leads to significant fluid flow in the sediment, with majority of the velocity being in the vertical (z) direction, particularly in the feeding column. There is also significant downward and horizontal velocity in the immediate vicinity of the feeding pocket, but these components of the velocity decrease quickly with increasing distance from the feeding pocket (for a visualization of such flow fields see Meysman et al. 2005). The injection of oxic overlying water into otherwise anoxic sediment porewater results in the formation of a volume of oxygenated sediment around the feeding pocket. Due to the higher permeability of the feeding column, the simulations show sediments directly above the feeding pocket that are more oxidized than the surrounding sediment (Fig. 1A). The upward advection caused oxygen penetration depths at the sediment-water interface (SWI) to be very small (less than 1 mm) and when high advection velocities are imposed, the oxic porewater from the burrow is ejected from the sediment to the overlying water. When oxygen is consumed rapidly relative to advection, lugworm-induced advective flow leads to the ejection of anoxic porewater (cf. results in Volkenborn et al. 2010). The input of nitrate at the injection pocket also stimulates denitrification, which extends from areas with low oxygen levels out into the anoxic zone (Fig. 1B).

Effects of burrowing and irrigation behavior

The model simulations show a clear impact of the amount of fluid pumped on depth-integrated rates of denitrification (Fig. 2). Higher flow rates, typically corresponding to larger organisms, lead to increased areal rates of denitrification; additionally, a decrease in the flow rate through the sediment diminishes the effect of feeding pocket depth on denitrification, especially in the case of slow rates of organic matter oxidation (k_{DOM} = 1 x 10^{-5} s^{-1}). In the case of environments with faster rates of organic matter oxidation, all nitrate injected into the sediment is consumed, so that denitrification increases linearly above rates of 1 mL min^{-1} up to the maximum irrigation rates reported for arenicolid polychates. Irrigation intensity also tends to increase rates of nitrification (Fig. 3), but because this coincides with a large increase in nitrate supply through the injection of burrow water, an increase in irrigation intensity lowers the proportion of denitrification coupled to nitrification (Fig. 4). When ammonium produced by actively respiring and excreting organisms is present in the burrow water (Kristensen et al. 1991), the initial dip in nitrification with increased pumping (Fig. 3) is not seen, as the oxidation of injected ammonium offsets the decrease in nitrification due to flushing of surficial sediments. Irrigation also alters the partitioning of oxygen consumption: increasing irrigation rates lead to a decrease in the overall proportion of oxygen consumed in oxidation of reduced metabolites as opposed to aerobic respiration, though there is a stimulation of the absolute rates of secondary metabolite oxidation. In the absence of irrigation (Q = 0 mL min^{-1}) oxidation of secondary metabolites can account for more than 50% of oxygen consumption. This percentage drops very quickly with increasing irrigation to ~20% at Q = 0.6 mL min^{-1} and ~11% at Q = 1.8 mL min^{-1} in our simulations. This is because irrigation introduces reactive DOM in addition to oxygen, and the precise partitioning of oxygen consumption is dependent on the ratio of oxygen to carbon in the burrow lumen fluid, even though the overall pattern of partitioning remains the same.

In addition to showing strong effects of irrigation intensity, reactive transport modeling reveals a substantial impact of burrow depth on sediment nitrogen cycling (Fig. 2). The effect of burrow depth depends on sediment organic matter reactivity, with faster organic matter breakdown diminishing the impact of feeding pocket depth on sediment denitrification. At low to intermediate oxygen consumption, indicative of sediments with relatively low organic matter content, deeper burrows lead to a higher predicted nitrification (and by extension, coupled denitrification) when compared to shallow burrows. However, faster rates of OM degradation lead to complete consumption of injected solutes regardless of burrow location, negating the effects of burrow depth seen in less reactive sediments (Figs. 2 and 3).

Importance of continuous versus discontinuous burrow irrigation

In simulations with slow organic matter mineralization, k_{DOM} = 10^{-5} s^{-1}, the volume of oxygenated sediment - here defined as [O_2] > 10 μM - is near-constant regardless of irrigation type (ranging from 244 cm^3 to 152 cm^3, depending on burrow depth), as the drawdown of oxygen is very slow relative to the time scale of pumping. However, faster rates of organic matter decomposition lead to pronounced oscillations of the oxygenated sediment volume. When the DOM oxidation rate constant is increased to 10^{-3} s^{-1}, the volume of sediment subject to oxic oscillation (defined as sediment that experiences [O_2] greater and smaller than 10 μM within a flushing cycle) is roughly 30 cm^3, which represents approximately 30% of the maximum oxic volume observed over a pumping cycle for the higher reactivity setting. This oxic oscillation due to intermittent pumping leads to temporally variable rates of nitrogen cycling and transport; however, the modeled time-integrated rates of nitrogen cycling for constant and intermittent pumping are indistinguishable under the conditions simulated, due to the complete consumption of injected solutes over the period of a pumping cycle.

Uncertainties in model formulation

Increasing the nitrification rate constant from k_{NH4} ~5 μM^{-1} yr^{-1} to ~500 μM^{-1} yr^{-1} (after the sensitivity analysis in Na et al. 2008) results in a roughly three-fold intensification in the areal rates of nitrification (from 0.2 to 0.62 mmol N m^{-2} d^{-1}) in models with high organic matter loading, and up to a five-fold increase in models with low OM (from 0.31 to1.52 mmol m^{-2} d^{-1}). The enhanced nitrification in turn stimulates denitrification, from 1.6 to 2.0 mmol N m^{-2} d^{-1} in models with high organic matter reactivity.

The depth distribution of particulate organic matter (POM) has a small effect on sediment nitrogen cycling, on the order of a 5% reduction in sediment denitrification when POM is uniform across depth as opposed to an exponential decay with increasing depth in the sediment: 1.65 mmol m^{-2} d^{-1} denitrification vs. 1.75 mmol m^{-2} d^{-1} for an irrigation rate of 1.5 mL min^{-1}. Uniform distribution of reactive POM, representative of heavily bioturbated sediments, increases the availability of POM at depth. However, this decreases the depth-integrated rates of both nitrification and denitrification because more O_2 is used for aerobic respiration rather than nitrification that fuels coupled denitrification.

Discussion

Model Validation

Model results show that pumping by a lugworm leads to distinct spatial structuring of concentration distributions, with injected solutes concentrated around a central feeding pocket (Fig. 1A). Calculated oxygen penetration depths at both the sediment-water interface and feeding pocket agree well with penetration depths measured using planar optodes in laboratory aquaria containing *Arenicola marina* – a species with similar behavior and irrigation patterns as *A. pacifica* (Woodin & Wethey, 2009) - and homogenized organic matter-rich (organic content = 1.5%) sediment (Timmermann et al. 2006, Volkenborn et al. 2010). Additionally, the computed horizontal pressure decay of $p(r) \sim r^{-1.12}$ for a single organism in an infinite domain is similar to the peak pressure decay observed in the field following a defecation event (Wethey et al. 2008), indicating that the modeled physics are consistent with observations.

In the simulations using the laboratory-derived organic matter degradation constant (k_{DOM} = 10^{-5} s^{-1}, based on sediment slurry incubations), advective transport is fast relative to the rate of oxygen and nitrate consumption, which leads to ejection of O_2-containing porewater from the sediment into the overlying water. However, faster rates of organic matter oxidation result in the ejection of net reduced porewater; the modeled ejection of porewater at the SWI compares favorably to oxygen optode data from Volkenborn et al. (2010) that also show ejection of anoxic porewater into the overlying water during phases of burrow irrigation (average irrigation rate = 0.2 – 2.6 mL min^{-1}). This flushing of porewater could serve as an important source of reduced substances – especially ammonium – for the overlying water and autotrophic communities at the sediment surface (Marinelli 1992).

Modeled nitrate fluxes are in good agreement with the microcosm data, though the model consistently underestimates total oxygen consumption and ammonium efflux compared to the microcosms (Table 3). Modeled fluxes also compare well with a study by Na et al. (2008), who reported ammonium fluxes out of the sediment of 1.1 ± 3.2 to 4.7 ± 7.9 mmol m^{-2} d^{-1} for acclimated *Arenicola marina* and mechanical mimics, respectively. Our modeled nitrate uptake also falls within their measured range (3.9 ± 4.6 and -3.2 ± 4.0 mmol m^{-2} d^{-1} for live worms and mimics, respectively). The mismatch between our measured and modeled oxygen and ammonium fluxes likely reflects processes at the sediment-water interface that are not fully reflected in the model. CT scans of the laboratory microcosms revealed a significant population of small meiofauna in the upper layers of the cores, which was not replicated in the model simulations. Consumption of oxygen and secretion of ammonium by meiofauna, as well as the bioirrigation caused by their shallow burrowing in the topmost sediment layer, can increase both the benthic oxygen uptake and efflux of ammonium. When these potential faunal effects are included as an enhanced diffusion coefficient ($D_{enhanced} = D$ x 10) and elevated aerobic respiration in the surface 1 cm layer (a ten-fold increase reflecting meiofauna respiration that was not captured in our slurry incubation), models predict higher oxygen consumption, ~30 mmol m^{-2} d^{-1}. Notably, because nitrate penetration depths exceed the depth of the zone inhabited by the meiofauna in the microcosms, the enhanced transport in the upper layer of sediment has relatively small impacts on the modeled nitrate supply, leading to a closer match between modeled and measured nitrate fluxes (Table 3).

Energetics of pumping

Although models are able to accurately recreate observed pressure signals with single organisms, pressure fields computed in multi-organism settings at a burrow density of 10 ind. m^{-2} exhibit a significantly smaller horizontal decay of the pressure signal (p(r) ~ r$^{-0.4}$) than burrows without nearby neighbors (p(r) ~ r-1.12), due to the influence of nearby pumping organisms. Despite this impact on pressure fields, the pumping power equation from Riisgard et al. (1996) – $P_p(Q) = \rho * g * \Delta H_p(Q) * Q$, where P_p is the energetic cost of pumping in Watts, Q is the volumetric flow rate, and $\Delta H_p(Q)$ is the sum of the pressure over the pump system and the imposed back pressure – shows that these variations result in minimal energetic costs to arenicolids (less than 1% of the total metabolism of a typical arenicolid; Riisgard et al. (1996)). The minimal metabolic effect of interacting pressure fields suggests that interactions between neighboring arenicolids are mediated by factors other than the energetic costs directly associated with burrow irrigation, such as increased food availability from increased downward surface deposit movement or localized depletion of food deposits due to the competitive feeding of multiple arenicolids (Longbottom 1970, Boldina & Beninger 2014).

The impacts of burrowing and irrigation behavior on nitrogen cycling

Burrowing depth and volumetric irrigation rate had major impacts on calculated nitrogen cycling (Figs. 2 and 3). Increases in the irrigation rate Q enhance denitrification (Fig. 2), especially in the case of deeper burrows; shallow burrows can offset the effects of increasing flow rate due to the ejection of reactive solutes. The impacts of irrigation intensity are also dependent on environmental context: at higher rates of organic matter breakdown (Fig. 2, diamonds, representing all simulated burrow depths between 5 and 15 cm), the increase in denitrification is linear above moderate flushing rates (1 mL min^{-1}) regardless of burrow depth. This linear relationship between denitrification and Q is because in highly reactive sediments with excess labile organic matter, denitrification is limited by the supply of nitrate from the overlying water (see e.g. Seitzinger et al. 2006). Furthermore, in highly reactive sediments, our model shows that nitrification tends to decrease with irrigation (Fig. 3), as oxygen is preferentially consumed via aerobic respiration of the injected DOM, rather than being used in nitrification, which is kinetically slower than aerobic respiration.

Burrow irrigation leads to a shift from SWI-dominated to deep feeding pocket-dominated denitrification. When Q is low, diffusive transport across the SWI is the dominant process supplying nitrate compared to advective supply from the feeding pocket, so the steeper concentration gradient in highly reactive sediments supports higher rates of denitrification relative to sediments with lower organic matter loading. Thus in poorly-irrigated, SWI-dominated sediments, organic matter availability and reactivity is a primary control on nitrogen cycling (Fig. 2), which agrees with previous empirical and modeling studies of denitrification (Berg et al. 2003, Lee et al. 2006). After an initial decline in nitrification related to flushing of surficial ammonium, both nitrification and denitrification increase with irrigation rates (Figs. 2 and 3). This represents a switch from a diffusion-dominated environment, where the SWI accounts for 75% of total denitrification, to one dominated by advective supply and nitrogen cycling associated with the feeding pocket. In the latter case, consumption associated with the feeding pocket accounts for more than 90% of denitrification at high irrigation rates. This is because irrigation introduces not only nitrate, but also oxygen and dissolved organic matter (Gardner et al. 1993), which is broken down into ammonium that supplies nitrification. Our modeled effects of irrigation intensity agree well with findings by Na et al. (2008) that similarly show an increase in both N_2 production as a function of Q, and a higher rate of nitrification in intensely irrigated microcosms relative to controls.

The model results suggest that system responses to changes in burrow depth are governed by changes in the time scales of competing processes within the domain, especially the residence time of the injected fluid (Fig. 5). In cases with rapid consumption of organic matter and corresponding complete consumption of oxygen and nitrate, feeding pocket depth has minimal effect on nitrogen cycling due to the complete consumption of nitrate before ejection across the SWI is possible. However, cases with incomplete consumption of nitrogen due to lower sediment reactivity lead to pronounced decreases in sediment denitrification for shallow relative to deep burrows (compare 5, 10, and 15cm depths in Fig. 2; dashed lines in Fig. 5). When nitrate produced through nitrification - as opposed to injected nitrate - is the dominant source for denitrification, feeding pocket depth is unimportant (Figs. 3 and 4 at low values of Q), because nitrogen produced *in situ* is rapidly consumed in denitrification regardless of burrow location.

Our results, particularly uncertainties in the model parameterization, highlight important knowledge gaps. The oxygen to DOM ratio in injected burrow water plays a critical part in determining the redox oscillation of the sediment and in turn the potential for nitrification and denitrification. When levels of oxygen exceed the available reactive reducing equivalent, the sediment around a feeding pocket remains oxidized, and denitrification rates are low due to a lack of reactive organic matter for use in denitrification. Alternatively, injected porewater with a DOM to O_2 ratio greater than 1 (an excess of DOM) creates oxygen distribution patterns that are more in line with observations that show areas of oxidized sediment closely associated with the feeding pocket but extending no more than 2-3 cm into the surrounding sediment (e.g., Volkenborn et al. 2010). Although oxygen levels in the burrow lumen and injected water are fairly well constrained (Volkenborn et al. 2010), there is scant information on the levels of labile organic material or nitrogen compounds in the burrow lumen. The assumed value of 115 μM C in the burrow water leads to modeled oxygen concentrations that closely match measured optode data, but the concentration of DOM nonetheless represents an important area of uncertainty. Our model results show that system responses to irrigation intensity are highly dependent on burrow water composition, so knowledge on the chemical makeup of burrow lumen water, which may differ from the overlying water due to microbial processes associated with the burrow lining, is critical to accurately predict infaunal effects on nitrogen cycling.

Benthic Context and Controls on Nitrogen Cycling

Extrapolating our predicted denitrification rates for individual organisms to the field scale using an organism density of 32 ind. m^{-2}, which is typical for a sand flat dominated by *A. marina* (Volkenborn et al. 2007b), leads to a maximum integrated denitrification potential of 25 mmol N m^{-2} d^{-1}. This is very high compared to commonly reported rates of <1 – 6 mmol N m^{-2} d^{-1} (Seitzinger 1988), suggesting that limits on nitrate supply to the anoxic sediment may prevent this maximum from being reached. This discrepancy may alternatively be due to the fact that some nitrogen flux measurements may not capture the effects of larger infauna due to the use of undisturbed cores for measurements (Cowan & Boynton 1996, Eyre & Ferguson 2002), even though the irrigation rates that are modeled here have pronounced effects on nitrogen cycling. Additionally, if larger infauna such as those modeled here produce relatively low-density burrow openings, their effect may not be captured if the size of the benthic flux chambers is small relative to inter-burrow distance; in this case, chambers with a diameter less than 10 cm would potentially miss burrow openings, especially if burrows are not distributed evenly (Dornhoffer et al. 2012). Individual variability in irrigation rate and – to a lesser extent – burrow depth may also explain at least in part the large variabilities in maximum denitrification rates that have been documented empirically (Stief 2013), further solidifying the importance of considering infauna when measuring and predicting system-wide rates of nitrogen reduction.

In most coastal environments with high organic matter loading, our results suggest that denitrification is controlled by irrigation intensity, which determines the availability of nitrate. On an areal basis, spatially integrated volumetric rates of biologically driven fluid exchange between sediment and the overlying water reflect both organisms' intrinsic irrigation rate and organism density. Our results suggest that increasing organism density will enhance sediment denitrification rates by increasing the areal irrigation rate. This is a possible mechanism leading both to observed density effects (Marinelli et al. 2003, Waldbusser & Marinelli 2009) and to species-specific effects (Norling et al. 2007), as irrigation behaviors are largely characteristic for given arenicolid species (Riisgard et al. 1996). Furthermore, changes in areal irrigation rate due to a species interaction response can be a potential mechanism underlying the effects of functional diversity on ecosystem function (Waldbusser & Marinelli 2006, Norling et al. 2007, Michaud et al. 2009).

Lugworm irrigation and nitrogen cycling

Irrigation intensity and burrowing depth are commonly related to organism size and thus age (Riisgard et al. 1996) suggesting that aging and subsequent changes in irrigation behavior can increase sediment denitrification substantially, up to 4 – 5 fold over non-irrigated sediments (Fig. 2). Our findings on the importance of burrow irrigation suggest that an environment being initially recolonized by infauna after a hypoxic event – represented in our models by an increase in the overall irrigation rate – may initially experience enhanced ammonium effluxes, followed by increased rates of nitrification (and thus a decreased efflux of ammonium). This change in nitrogen cycling is because opportunistic pioneer organisms both increase in number and increase in age, creating deeper, more intensely irrigated burrows. The enhanced supply of nitrate from the overlying water via irrigation will rapidly increase denitrification, decreasing the proportion of coupled nitrification-denitrification (Fig. 4). This is precisely the pattern seen by Bartoli et al. (2000) in a microcosm simulation of the initial stages of such a recolonization event.

The importance of discontinuous irrigation

When sediment reactivity is low, the slow consumption of oxygen relative to the frequency of irrigation periods leads to minimal oscillation in oxic volume. However, as the reactivity of organic matter is increased, model simulations exhibit pronounced redox oscillation in sediment surrounding the feeding pocket (not shown), consistent with the analysis of Volkenborn et al. (2012) and the oxygen dynamics caused by the pumping of *Arenicola marina* documented in Volkenborn et al. (2010). Our results expand on these findings and show that the redox oscillation unsurprisingly leads to oscillations in nitrogen fluxes and instantaneous nitrification and denitrification rates, reflecting the redox-sensitive nature of these reactions and movement of the oxic-anoxic interfaces.

Despite the observed temporal variability, the time-averaged areal nitrogen cycling rates appear to be largely independent of irrigation pattern. In the model, these rates are independent of irrigation pattern because in the models that produce significant fluctuations in redox conditions (k = 10^{-3} s^{-1}), all injected nitrate and oxygen is consumed. This contrasts with findings documenting a distinct change in porewater ammonium concentrations and organic matter degradation rates due to redox oscillation (Aller et al. 1994, Sun et al. 2002), but that effect has been observed as a result of days-scale oscillations, rather than the minute-scale considered here. In our model, the microbial community is assumed to be at a steady state in terms of size and composition, and rate constants used to parameterize the reaction network reflect a (uniform) reaction potential, wherein process rates are modulated only by the distribution of substrates. However, redox oscillation likely causes shifts in microbial community composition and activity that are not considered in our approach. It is also possible that environmental conditions at the minute scale are too fast to elicit a strong microbial response, such that high frequency redox oscillations cease to be an important consideration. We are not aware of published data that addresses this potentially important issue impacting benthic nitrogen fluxes.

Conclusions

Variations in the feeding pocket depth and burrow irrigation rate of lugworms can have substantial effects on nitrogen cycling in the vicinity of individual burrows. Increasing the amount of nitrate provided through irrigation activity stimulates denitrification, yet shallow feeding pockets can lead to ejection of burrow lumen fluid out of the sediment before consumption of reactive solutes is complete. Although discontinuous irrigation leads to distinct temporal variability within the sediment, the time-averaged rates of nitrogen cycling differ minimally from a case of continuous irrigation. However, this model finding does not take into consideration the response of the microbial community to redox oscillations, a feedback which could account for changes in nitrogen cycling rates that have been observed in empirical studies at the individual scale. Finally, our results suggest that variations in organism behavior such as burrow irrigation are an additional aspect of the benthic community that must be taken into account to predict ecosystem function, as well as possibly being one mechanism to explain the observed relationships between species diversity and system function.

Acknowledgements. This publication was supported by the National Science Foundation (OCE 0751882 to C.M. and OCE 1014226 to G.G.W.). Additional support was received from the Gulf of Mexico Research Initiative Ecological Impacts of Oil and Gas Inputs to the Gulf to C.M. This is ECOGIG contribution no. 358 and the benthic flux data reflect GRIIDC accession number R4.x268.183:0001. We thank the reviewers for their insightful feedback that helped to improve the manuscript.

References

Aller, R.C. 1994. Bioturbation and remineralization of sedimentary organic matter: effects of redox oscillation. Chemical Geology 114: 331-345

Aller, R.C. and J.Y. Aller. 1998. The effect of biogenic irrigation intensity and solute exchange on diagenetic reaction rates in marine sediments. J Mar Res 56: 905-936

Aller, R.C. 2001. Transport and reactions in the bioirrigated zone. In Boudreau, B.P. and B.B. Jorgensen (eds). The benthic boundary layer: transport processes and biogeochemistry. Oxford University Press, Oxford, p. 269 - 301

Alperin, M.J., C.S. Martens, D.B. Albert, I.B. Suayah, L.K. Benninger, N.E. Blair, and R.A. Jahnke. 1999. Benthic fluxes and porewater concentration profiles of dissolved organic carbon in sediments from the North Carolina continental slope. Geochim Cosmochim Acta 63: 427-448

An, S., and W.S. Gardner. 2002. Dissimilatory nitrate reduction to ammonium (DNRA) as a nitrogen link, versus denitrification as a sink in a shallow estuary (Laguna Madre/Baffin Bay, Texas). Mar Ecol Prog Ser 237: 41-50

Banta, G.T., M. Holmer, M.H. Jensen, and E. Kristensen. 1999. Effects of two polychaete worms, *Nereis diversicolor* and *Arenicola marina*, on aerobic and anaerobic decomposition in a sandy marine sediment. Aquat Microb Ecol 19: 189-204

Bartoli, M., D. Nizzoli, D.T. Welsh, and P. Viaroli. 2000. Short-term influence of recolonisation by the polychaete worm *Nereis succina* on oxygen and nitrogen fluxes and denitrification: a microcosm simulation. Hydrobiologia 431: 165-174

Bars, M.L., and M.G. Worster. 2006. Interfacial conditions between a pure fluid and a porous medium: implications for binary alloy solidification. J Fluid Mech 550: 149 - 173

Berg, P., S. Rysgaard, P. Funch, and M.K. Sejr. 2001. Effects of bioturbation on solutes and solids in marine sediments. Aquat Microb Ecol 26:81-94

Berg, P., S. Rysgaard, and B. Thamdrup. 2003. Dynamic modeling of early diagenesis and nutrient cycling. A case study in an arctic marine sediment. Am J Sci 303: 905 – 955

Boldina, I. and P.C. Beninger. 2014. Fine-scale spatial distribution of the common lugworm *Arenicola marina*, and effects of intertidal clam fishing. Est Coast Shelf Sci 143: 32 - 40

Boudreau, B.P. 2001. Solute transport above the sediment-water interface. In: Boudreau, B.P. and B.B. Jorgensen (eds). The benthic boundary layer: transport processes and biogeochemistry. Oxford University Press, Oxford, p. 104-126

Canfield, D.E., A.N. Glazer, and P.G. Falkowski. 2010. The evolution and future of Earth's nitrogen cycle. Science 330: 192 – 196

Christensen, P.B., S. Rysgaard, N.P. Sloth, T. Dalsgaard, and S. Schwaerter. 2000. Sediment mineralization, nutrient fluxes, denitrification and dissimilatory nitrate reduction to ammonium in an estuarine fjord with sea cage trout farms. Aquat Microb Ecol 21: 73 - 84

Chung, J. and GM Hulbert. 1993. A time integration algorithm for structural dynamics with improved numerical dissipation – the generalized alpha method. J Appl Mech -Transactions of the ASME 60: 371-375

Cloern, J.E. 2001. Our evolving conceptual model of the coastal eutrophication problem. Mar Ecol Prog Ser 210: 223-253

Cowan, J.L.W., and W.R. Boynton. 1996. Sediment-water oxygen and nutrient exchanges along the longitudinal axis of Chesapeake Bay: seasonal patterns, controlling factors and ecological significance. Estuaries 19: 562 - 580

D'Andrea, A.F., R.C. Aller, and G.R. Lopez. 2002. Organic matter flux and reactivity on a South Carolina sandflat: the impacts of porewater advection and macrobiological structures. Limnol Oceanogr 47: 1056 – 1070

D'Andrea, A.F. and T.H. DeWitt. 2009. Geochemical ecosystem engineering by the mud shrimp *Upogebia pugettensis* (Crustacea: Thalassinidae) in Yaquina Bay, Oregon: density-dependent effects on organic matter remineralization and nutrient cycling. Limnol Oceanogr 54: 1922 – 1932

Dalsgaard, T., B. Thamdrup, and D.E. Canfield. 2005. Anaerobic ammonium oxidation (anammox) in the marine environment. Res Microbiol 156: 457 - 464

Diaz, R.J. and R. Rosenberg. 2008. Spreading dead zones and consequences for marine ecosystems. Science 321: 926 – 929

Dornhoffer, T.M., G.G. Waldbusser, and C. Meile. 2012. Burrow patchiness and oxygen fluxes in bioirrigated sediments. J Exp Mar Biol Ecol 412: 81 - 86

Emmerson, M.C., M. Solan, C. Emes, D.M. Paterson, and D. Raffaelli. 2001. Consistent patterns and the idiosyncratic effects of biodiversity in marine ecosystems. Nature 411: 73-77

Engstrom, P., T. Dalsgaard, S. Hulth, and R.C. Aller. 2005. Anaerobic ammonium oxidation by nitrite (annamox): implications for N_2 production in coastal marine sediments. Geochim Cosmochim Acta 69: 2057-2065

Eyre, B.D., and A.J.P. Ferguson. 2002. Comparison of carbon production and decomposition, benthic nutrient fluxes and denitrification in seagrass, phytoplankton, benthic microalgae- and macroalgae-dominated warm-temperature Australian lagoons. Mar Ecol Prog Ser 229: 43 - 59

Fornes, W.L., D.J. DeMaster, L.A, Levin, and N.E. Blair. 1999. Bioturbation and particle transport in Carolina slope sediments: a radiochemical approach. J Mar Res 57: 335-355

Galloway, J.N., F.J. Dentener, D.G. Capone, E.W. Boyer, R.W. Howarth, S.P. Seitzinger, G.P. Asner, C.C. Cleveland, P.A. Green, E.A. Holland, D.M. Karl, A.F. Michaels, J.H. Porter, A.R. Townsend, and C.J. Vorosmarty. 2004. Nitrogen cycles: past, present, and future. Biogeochemistry 70: 153 - 226

Gardner, W.S., E.E. Briones, E.C. Kaegi, and G.T. Rowe. 1993. Ammonium excretion by benthic invertebrates and sediment-water nitrogen flux in the Gulf of Mexico near the Mississippi River outflow. Estuaries 16: 799-808

Gardner, W.S., M.J. McCarthy, S. An, D. Sobolev, K.S. Sell, and D. Brock. 2006. Nitrogen fixation and dissimilatory nitrate reduction to ammonium (DNRA) support nitrogen dynamics in Texas estuaries. Limnol Oceanogr 51: 558-568

Gilbert, F., R.C. Aller, and S. Hulth. 2003. The influence of macrofaunal burrow spacing and diffusive scaling on sedimentary nitrification and denitrification: an experimental simulation and model approach. J Mar Res 61: 101-125

Henriksen, K., M.B. Rasmussen, and A. Jensen. 1983. Effect of bioturbation on microbial nitrogen transformations in the sediment and fluxes of ammonium and nitrate to the overlying water. Environmental Biogeochemistry 35: 193-205

Huettel, M. 1990. Influence of the lugworm *Arenicola marina* on porewater nutrient profiles of sand flat sediments. Mar Ecol Prog Ser 62:241-248

Kemp, W.M., W.R. Boynton, J.E. Adolf, D.F. Boesch, W.C. Boicourt, G. Brush, J.C. Cornwell, T.R. Fisher, P.M. Gilbert, J.D. Hagy, L.W. Harding, E.D. Houde, D.G. Kimmel, W.D. Miller, R.I.E. Newell, M.R. Roman, E.M. Smith, and J.C. Stevenson. 2005. Eutrophication of Chesapeake Bay: historical trends and ecological interactions. Mar Ecol Prog Ser 303: 1 - 29

Koop-Jakobsen, J., and A.E. Giblin. 2010. The effect of increased nitrate loading on nitrate reduction via denitrification and DNRA in salt marsh sediments. Limnol Oceanogr 55: 789-802

Kristensen, E., and T.H. Blackburn. 1987. The fate of organic carbon and nitrogen in experimental marine sediment systems: influence of bioturbation and anoxia. J Mar Res 45: 231-257

Kristensen, E., M.H. Jensen, and R.C. Aller. 1991. Direct measurement of dissolved inorganic nitrogen exchange and denitrification in individual polychaete (*Nereris virens*) burrows. J Mar Res 49: 355 - 377

Kuhl, M. and B.B. Jorgensen. 1992. Microsensor measurements of sulfate reduction and sulfide oxidation in compact microbial communities of aerobic biofilms. Appl Env Microbiol 58: 1164-1174

Lam, P. and M.M.M. Kuypers. 2011. Microbial nitrogen cycling processes in oxygen minimum zones. Annu Rev Mar Sci 3: 317 – 345

Lee, R. and S.B. Joye. 2006. Seasonal patterns of nitrogen fixation and denitrification in oceanic mangrove habitats. Mar Ecol Prog Ser 307: 127 - 141

Levin, L.A., W. Ekau, A.J. Gooday, F. Jorissen, J.J. Middelburg, S.W.A. Naqvi, C. Neira, N.N. Rabalais, and J. Zhang. 2009. Effects of natural and human-induced hypoxia on costal benthos. Biogeosciences 6: 2063 – 2098

Longbottom, M.R. 1970. The distribution of *Arenicola marina (L.)* with particular reference to the effects of particle size and organic matter of the sediments. J Exp Mar Biol Ecol 5: 138 - 157

Marinelli, R.L. 1992. Effects of polychaetes on silicate dynamics and fluxes in sediments: importance of species, animal activity, and polychaete effects on benthic diatoms. J Mar Res 50: 745-779

Marinelli, R.L. and B.P. Boudreau. 1996. An experimental and modeling study of pH and related solutes in an irrigated anoxic coastal sediment. J Mar Res 54: 939 - 966

Marinelli, R.L. and T.J. Williams. 2003. Evidence for density-dependent effects of infauna on sediment biogeochemistry and benthic-pelagic coupling in nearshore systems. Est Coast Shelf Sci 57: 179-192.

Meysman, F.J.R., O.S. Galaktionov, and J.J. Middelburg. 2005. Irrigation patterns in permeable sediments induced by burrow ventilation: a case study of *Arenicola marina*. Mar Ecol Prog Ser 303: 195 - 212

Meysman, F.J.R., O.S. Galaktionov, B. Gribsholt, and J.J. Middelburg. 2006. Bio-irrigation in permeable sediments: an assessment of model complexity. J Mar Res 64: 589-627

Michaud, E., G. Desrosiers, R.C. Aller, F. Mermillod-Blondin, B. Sundby and G. Stora. 2009. Spatial interactions in the *Macoma balthica* community control biogeochemical fluxes at the sediment-water interface and microbial abundances. J Mar Res 67:43-70.

Na, T., B. Gribsholt, O.S. Galaktionov, T. Lee, and F.J.R. Meysman. 2008. Influence of advective bio-irrigation on carbon and nitrogen cycling in sandy sediments. J Mar Res 66:691-722

Norling, K., R. Rosenberg, S. Hulth, A. Gremare, and E. Bonsdorff. 2007. Importance of functional biodiversity and species-specific traits of benthic fauna for ecosystem functions in marine sediment. Mar Ecol Prog Ser 332: 11-23

Pearl, H.W. and M.P. Piehler 2008. Nitrogen and Marine Eutrophication. In: D.G. Capone, D.A. Bronk, M.R. Mulholland and E.J. Carpenter (eds.) Nitrogen in the Marine Enviornment 2nd edition. Elsevier, Amsterdam. p. 529-568

Porubsky, W.P., S.B. Joye, W.S. Moore, K. Tuncay, and C. Meile. 2011. Field measurements and modeling of groundwater flow and biogeochemistry at Moses Hammock, a backbarrier island on the Georgia coast. Biogeochemistry 104: 69 - 90

Retraubun, A.S.W., M. Dawson, and S.M. Evans. 1996. The role of the burrow feeding funnel in feeding processes in the lugworm *Arenicola marina (L.)*. J Exp Mar Biol Ecol 202:107-118

Riedel, B., T. Pados, K. Pretterebner, L. Schiemer, A. Steckbauer, A. Haselmair, M. Zuschin, and M. Stachowitsch. 2014. Effect of hypoxia and anoxia on invertebrate behavior: ecological perspectives from species to community level. Biogeosciences 11: 1491 - 1518

Riisgard, H.U., I. Bernsten, and B. Tarp. 1996. The lugworm (*Arenicola marina*) pump: characteristics, modeling and energy cost. Mar Ecol Prog Ser 138: 149-156

Santos, I.R., B.D. Eyre, and R.N. Glud. 2012. Influence of porewater advection on denitrification in carbonate sands: evidence from repacked sediment column experiments. Geochim Cosmochim Acta 96: 247 - 258

Seitzinger, S.P. 1988. Denitrification in freshwater and coastal marine ecosystems: ecological and geochemical significance. Limnol Oceanogr 33: 702-724

Seitzinger, S., J.A. Harrison, J.K. Bohlke, A.F. Bouwman, R. Lowrance, B. Peterson, C. Tobias, and G. Van Drecht. 2006. Denitrification across landscapes and waterscapes: a synthesis. Ecol Appl 16: 2064 - 2090

Stief, P. 2013. Stimulation of microbial nitrogen cycling in aquatic ecosystems by benthic macrofauna: mechanisms and implications. Biogeosciences 10: 7829-7846

Sun, M.-Y., R.C. Aller, C. Lee, and S.G. Wakeham. 2002. Effects of oxygen and redox oscillation on degradation of cell-associated lipids in surficial marine sediments. Geochim Cosmochim Acta 66: 2003-2012

Sundbaeck, K., F. Linares, F. Larsen, and A. Wulff. 2004. Benthic nitrogen fluxes along a depth gradient in a microtidal fjord: the role of denitrification and microphytobenthos. Limnol Oceanogr 49: 1095-1107

Thamdrup, B., and T. Dalsgaard. 2002. Production of N_2 through anaerobic ammonium oxidation coupled to nitrate reduction in marine sediments. Appl Environ Microb 68: 1312 - 1318

Thamdrup, B. 2012. New pathways and processes in the global nitrogen cycle. Annu Rev Ecol Evol Syst 43: 407-428

Timmermann, K., G.T. Banta, and R.N. Glud. 2006. Linking *Arenicola marina* irrigation behavior to oxygen transport and dynamics in sandy sediments. J Mar Res 64:915-938

Van Cappellen, P., and Y. Wang. 1996. Cycling of iron and manganese in surface sediments: a general theory for the coupled transport and reaction of carbon, oxygen, nitrogen, sulfur, iron, and manganese. Am J Sci 296: 197-243

Volkenborn, N., L. Polerecky, S.I.C. Hedtkamp, J.E.E. van Beusekom, and D. de Beer. 2007a. Bioturbation and bioirrigation extend the open exchange regions in permeable sediments. Limnol Oceanogr 52: 1898-1909

Volkenborn, N., and K. Reise. 2007b. Effects of *Arenicola marina* on polychaete functional diversity revealed by large-scale experimental lugworm exclusion. J Mar Res 57: 78-88

Volkenborn, N., L. Polerecky, D.S. Wethey, and S.A. Woodin. 2010. Oscillatory porewater bioadvection in marine sediments induced by hydraulic activities of *Arenicola marina*. Limnol Oceanogr 55:1231-1247

Volkenborn, N., C. Meile, L. Polerecky, C.A. Pildtich, A. Norkko, J. Norkko, J.E. Hewitt, S.F. Thrush, D.S. Wethey, and S.A. Woodin. 2012. Intermittent bioirrigation and oxygen dynamics in permeable sediments: an experimental and modeling study of three tellinid bivalves. J Mar Res 70: 794-823

Waldbusser, G.G., R. L. Marinelli, R.B. Whitlach, and P.T. Visscher. 2004. The effects of infaunal biodiversity on biogeochemistry of coastal marine sediments. Limnol Oceanogr 49:1482-1492

Waldbusser, G.G., and R.L. Marinelli. 2006. Macrofaunal modification of porewater advection: role of species function, species interaction, and kinetics. Mar Ecol Prog Ser 311: 217 - 231

Waldbusser, G.G., and R.L. Marinelli. 2009. Evidence of infaunal effects on porewater advection and biogeochemistry in permeable sediments: a proposed infaunal functional group framework. J Mar Res 67: 503-532

Wethey, D.S., S.A. Woodin, N. Volkenborn, and K. Reise. 2008. Porewater advection by hydraulic activities of lugworms, *Arenicola marina*: a field, laboratory, and modeling study. J Mar Res 66: 255 - 273

Woodin, S.A., and D.S. Wethey. 2009. Arenicolid behaviors: similarity of *Arenicola marina* and *Abarenicola pacifica*. Zoosymposia 2: 447-456

Zhang, J., D. Gilbert, A.J. Gooday, L. Levin, S.W.A. Naqvi, J.J. Middelburg, M. Scranton, W. Ekau, A. Pena, B. Dewitte, T. Oguz, P.M.S. Monteiro, E. Urban, N.N. Rabalais, V. Ittekkot, W.M. Kemp, O. Ulloa, R. Elmgren, E. Escobar-Briones, and A.K. Van der Plas. 2010. Natural and human-induced hypoxia and consequences for coastal areas: synthesis and future development. Biogeosciences 7: 1443 - 1467

Figure Legends

Figure 1: Radial cross section of modeled distribution of oxygen concentrations (**A**) and rate of denitrification (**B**) within the sediment around a 15-cm deep feeding pocket in low reactivity sediment (k_{DOM} = 10^{-5} s^{-1}) and under continuous irrigation. The top 2 cm is the water overlying the sediment, and contour lines are the oxygen concentration (in mol m^{-3}) and the $\log_{10}$ of denitrification rates, respectively.

Figure 2: Depth-integrated denitrification rates as a function of irrigation rate, Q (continuous irrigation). In models with high organic matter lability (k_{DOM} = 1 x 10^{-3} s^{-1}), denitrification is independent of burrow depth, so diamonds with solid lines indicate all burrow depths; Triangles, circles and squares with dashed lines represent feeding pockets at 15, 10 and 5 cm depth, respectively, for an organic matter degradation rate constant value of k_{DOM} = 1 x 10^{-5} s^{-1}. Filled symbols indicate SWI-dominated systems (the percentage of denitrification in the upper 1 cm > 50% of total denitrification), and open symbols indicate models dominated by the burrow feeding pocket.

Figure 3: Calculated nitrification rates as a function of burrow irrigation intensity. Dashed lines represent k_{DOM} = 10^{-5} s^{-1} and solid lines indicate k= 10^{-3} s^{-1}. Triangles indicate 15 cm burrow depth, circles indicate 10 cm, and squares indicate 5 cm. Note that diamonds represent all depths for k_{DOM} = 10^{-3} s^{-1} because all burrow depths generate identical results. Filled symbols indicate conditions in which surface sediments dominate nitrification (the percentage of nitrification in the top 1 cm > 50% of total nitrification), and open symbols indicate a burrow-dominated environment.

Figure 4: Percentage of total denitrification that is supported by coupled nitrification (defined as nitrate produced in nitrification divided by the amount consumed in denitrification) as a function of irrigation intensity Q. Dashed lines indicate sediments with low organic matter reactivity, with squares, circles, and triangles representing 5 cm, 10 cm, and 15 cm deep feeding pockets, respectively. The solid black diamonds indicate all burrow depths in sediments with high organic matter reactivity.

Figure 5: Calculated denitrification as a function of transport time (defined as the burrow depth times the microcosm area, divided by the volumetric flow rate). Dashed lines indicate k_{DOM} = 1 x 10^{-5} s^{-1}, solid lines indicate k_{DOM} = 1 x 10^{-3} s^{-1}, triangles indicate a 15 cm burrow depth, circles indicate 10 cm, and squares represent burrows at 5 cm depth. Note that in low-k_{DOM} sediments, predicted denitrification rates are lower for vigorously irrigated shallow burrows (dashed line with squares) relative to deeper burrows, indicative of ejection of reactive nitrogen into the overlying water.

Table 1: Reactions and rate laws; subscripts *x* and *y* describe the composition of the organic matter and are set to 106 and 16, respectively.

Reaction	Equation	Expression
Aerobic DOM degradation (R1)	$(CH_2O)_x(NH_3)_y + xO_2 + yH^+ \rightarrow xCO_2 + yNH_4^+ + xH_2O$	k_{DOM}*DOM*O_2/(O_2+K_{mO2})
Denitrification (R2)	$(CH_2O)_x(NH_3)_y + \frac{4x}{5}(NO_3^-) + (\frac{4x}{5} + y)H^+ \rightarrow xCO_2 + yNH_4^+ + \frac{2x}{5}N_2 + \frac{7x}{5}H_2O$	(k_{DOM}*DOM-R1)*NO_3^-/(NO_3^- +K_{mNO3})
Iron Reduction (R3)	$(CH_2O)_x(NH_3)_y + 4xFe(OH)_3 + (8x+y)H^+ \rightarrow xCO_2 + yNH_4^+ + 4x\,Fe^{+2} + 11x\,H_2O$	((k_{DOM}*DOM-R1-R2)* $Fe(OH)_3$)/($Fe(OH)_3$ +$K_{mFe(OH)3}$)
Sulfate Reduction	$(CH_2O)_x(NH_3)_y + \frac{x}{2}SO_4^{2-} + (\frac{x}{2} + y)H^+ \rightarrow xCO_2 + yNH_4^+ + \frac{x}{2}HS^- + xH_2O$	(k_{DOM}*DOM-R1-R2-R3)*SO_4^{2-} /(SO_4^{2-}+K_{mSO4})
Nitrification	$NH_4^+ + 2O_2 \rightarrow NO_3^- + 2H^+ + H_2O$	k_{NH4}*NH_4^+*O_2
Sulfide Oxidation	$H_2S + 2O_2 \rightarrow SO_4^{2-} + 2H^+$	k_{HS}*HS^-*O_2
Iron Oxidation	$Fe^{2+} + \frac{1}{4}O_2 + \frac{5}{2}H_2O \rightarrow Fe(OH)_3 + 2H^+$	k_{Fe}*Fe^{2+}*O_2
Iron Precipitation	$Fe^{2+} + HS^- \rightarrow FeS + H^+$	k_{precip}* (Fe^{2+} * HS^-/(K_{FeS}*H^+)-1)
POM degradation	POM $\rightarrow$ DOM	k_{POM} * POM

Table 2: Parameters used in the reactive transport model and their respective sources.

Parameter	Description	Value	Units	Source
$O2_0$	Oxygen in the overlying water	0.22	mol m^{-3}	This Study
$O2_{inj}$	Oxygen injected across the feeding pocket	0.088	mol m^{-3}	Volkenborn et al. 2010
$NO3_0$	Nitrate in the overlying water	0 - 0.02	mol m^{-3}	This Study
DOM_{inj}	DOM injected across feeding pocket	0 - 0.115	mol m^{-3}	Alperin et al. 1999
k_{DOM}	Rate constant for DOM degradation	1×10^{-5} – 1×10^{-3}	s^{-1}	This Study
k_{POM}	Rate constant for POM degradation to DOM	1×10^{-8}	s^{-1}	This Study
k_{NH4}	Rate constant for nitrification	1.59×10^{-4} - 1.59×10^{-2}	(mol m^{-3})$^{-1}$ s^{-1}	Na et al. 2008
k_{HS}	Rate constant for sulfide oxidation	5.1×10^{-5}	(mol m^{-3})$^{-1}$ s^{-1}	Van Cappellen and Wang 1996
k_{Fe}	Rate constant for iron oxidation	3.17×10^{-4}	(mol m^{-3})$^{-1}$ s^{-1}	Van Cappellen and Wang 1996
K_mO_2	Half-saturation for oxygen	0.02	mol m^{-3}	Van Cappellen and Wang 1996
K_mNO_3	Half-saturation for nitrate	0.005	mol m^{-3}	Van Cappellen and Wang 1996
$K_mFe(OH)_3$	Half-saturation for iron oxides*	8.75×10^{-2}	mol m^{-3}	Van Cappellen and Wang, 1996
$K_mSO_4^{2-}$	Half-saturation for sulfate	0.03	mol m^{-3}	Kuhl and Jorgensen 1992
K_{FeS}	Solubility constant for FeS	$10^{-2.95}$	mol m^{-3}	Van Cappellen and Wang 1996
k_{precip}	Precipitation constant for FeS	1.9×10^{-9}	s^{-1}	Van Cappellen and Wang, 1996

* This half-saturation constant is more than two orders of magnitude lower than the iron oxide concentration estimated for our site, resulting in 0 order kinetics for dissimilatory iron reduction.

Table 3: Laboratory and model fluxes of nitrate, ammonium, and oxygen (mean and standard deviation). Positive fluxes are into the sediment.

	Oxygen (mmol m^{-2} d^{-1})	Nitrate (mmol m^{-2} d^{-1})	Ammonium (mmol m^{-2} d^{-1})
Measured*	**52.62 ± 3.29**	**1.46 ± 0.15**	**-3.40 ± 0.51**
Modeled			
***Q* = 1.6 mL min^{-1}**	**16.11**	**1.45**	**-1.57**
Q = 1.6 mL min^{-1}, with meiofauna**	**31.26**	**1.62**	**-2.60**
Q = 1.0 mL min^{-1}	**10.67**	**0.90**	**-1.26**
Q = 2.0 mL min^{-1}	**19.66**	**1.77**	**-1.73**

* Experimental microcosms contained meiofauna whose presence potentially impacted measured oxygen and nitrogen fluxes but were not included in model simulations.

** See text for details

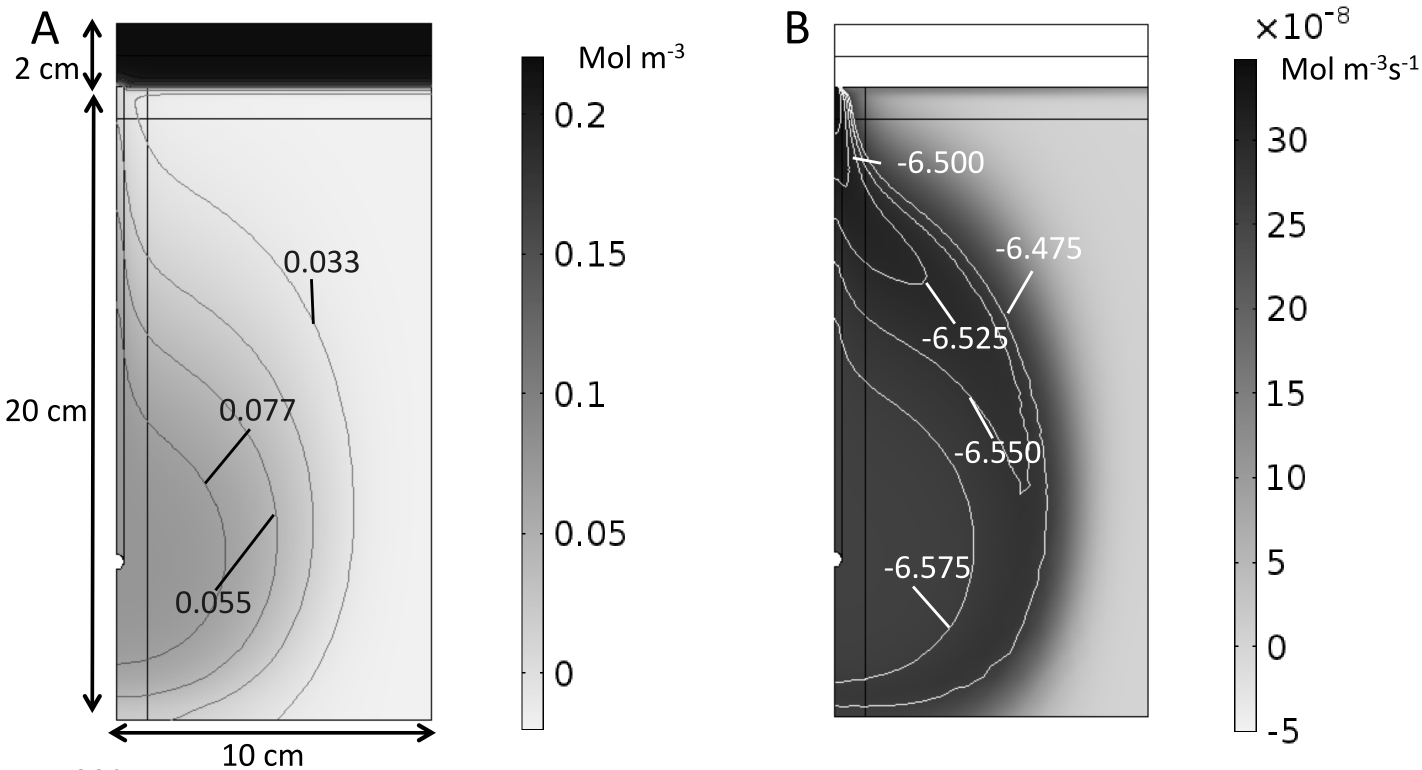
A
2 cm
20 cm
10 cm
0.033
0.077
0.055
Mol m-3
0.2
0.15
0.1
0.05
0
B
-6.500
-6.475
-6.525
-6.550
-6.575
×10-8
Mol m-3s-1
30
25
20
15
10
5
0
-5

Figure 1

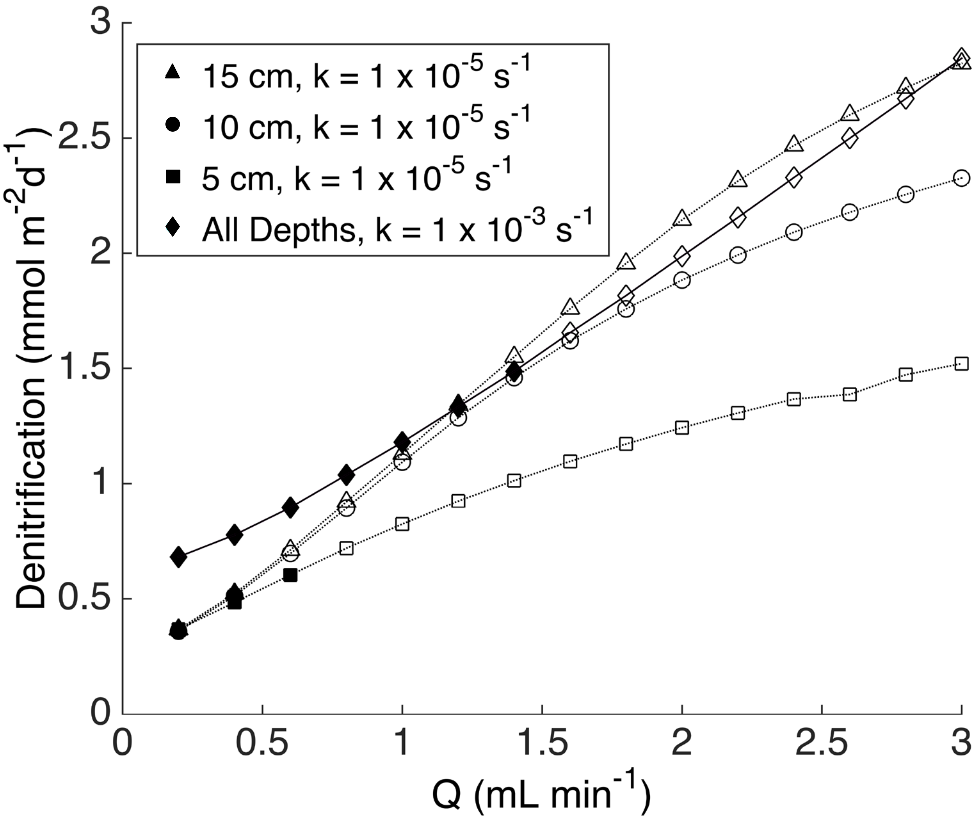
15 cm, k = 1 x 10^-5 s^-1
10 cm, k = 1 x 10^-5 s^-1
5 cm, k = 1 x 10^-5 s^-1
All Depths, k = 1 x 10^-3 s^-1
Denitrification (mmol m^-2 d^-1)
Q (mL min^-1)
0
0.5
1
1.5
2
2.5
3

Figure 2

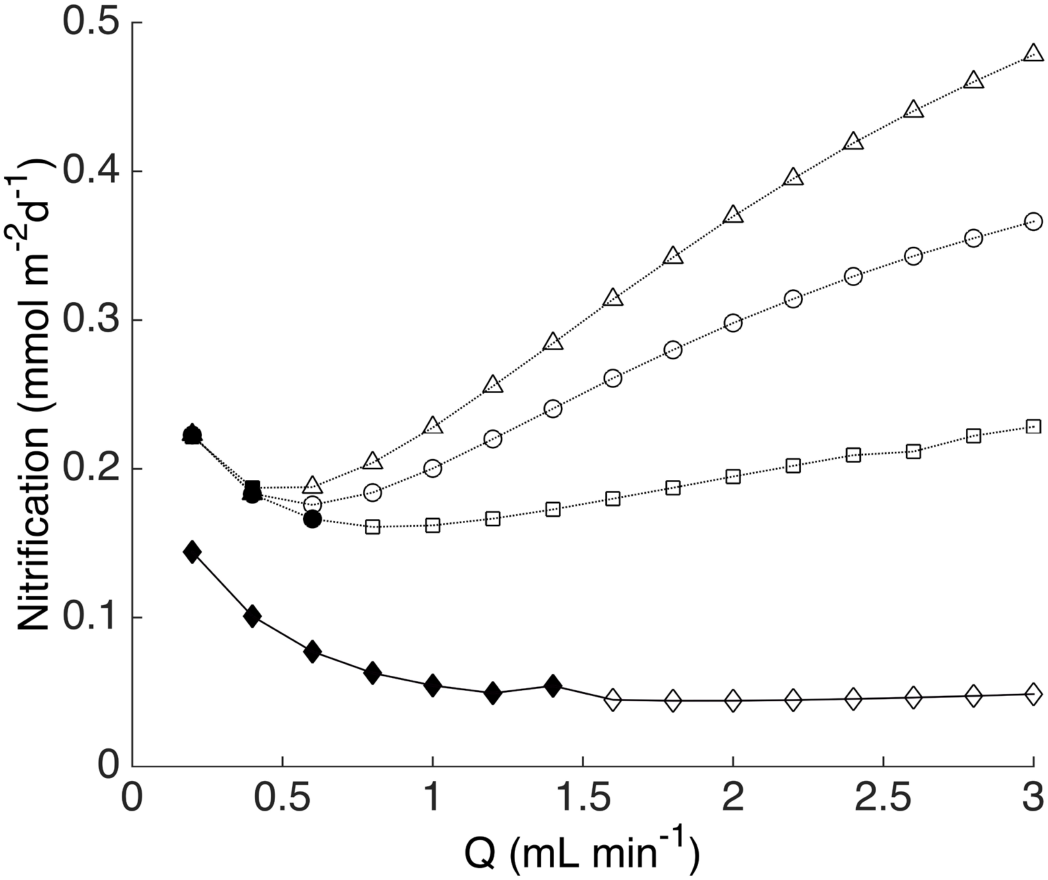

Figure 3

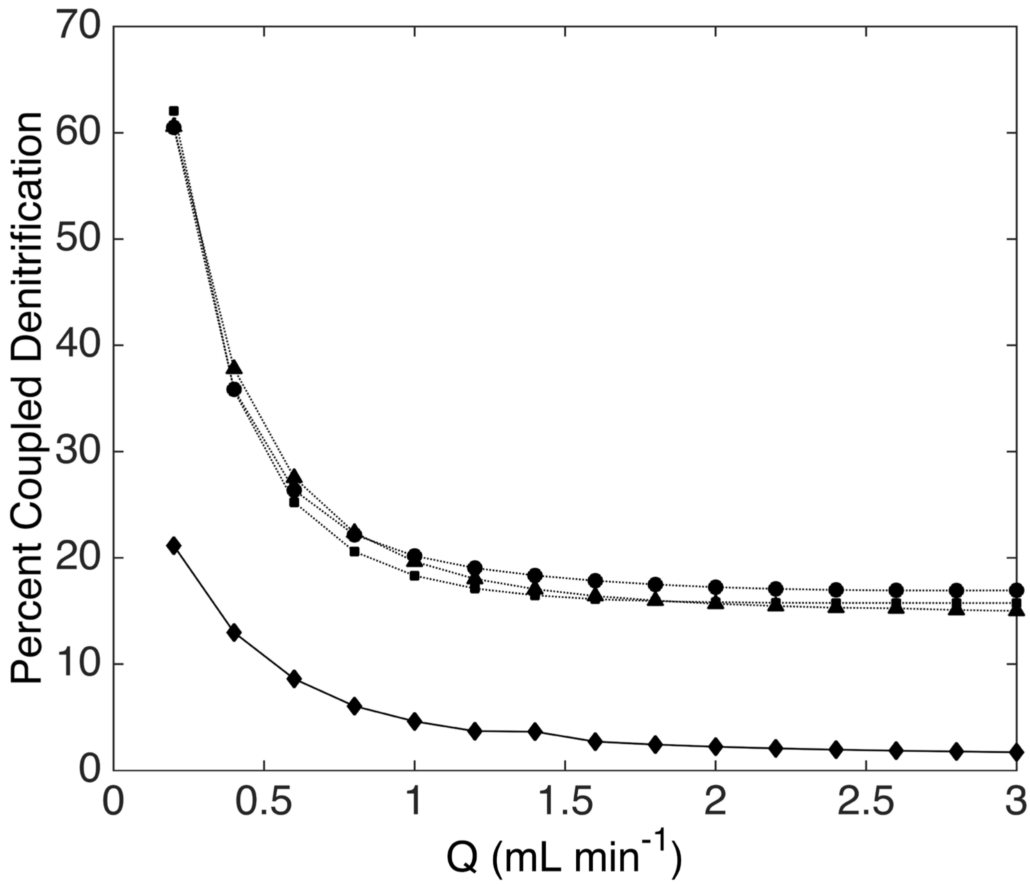
Percent Coupled Denitrification
Q (mL min-1)
0
10
20
30
40
50
60
70
0
0.5
1
1.5
2
2.5
3

Figure 4

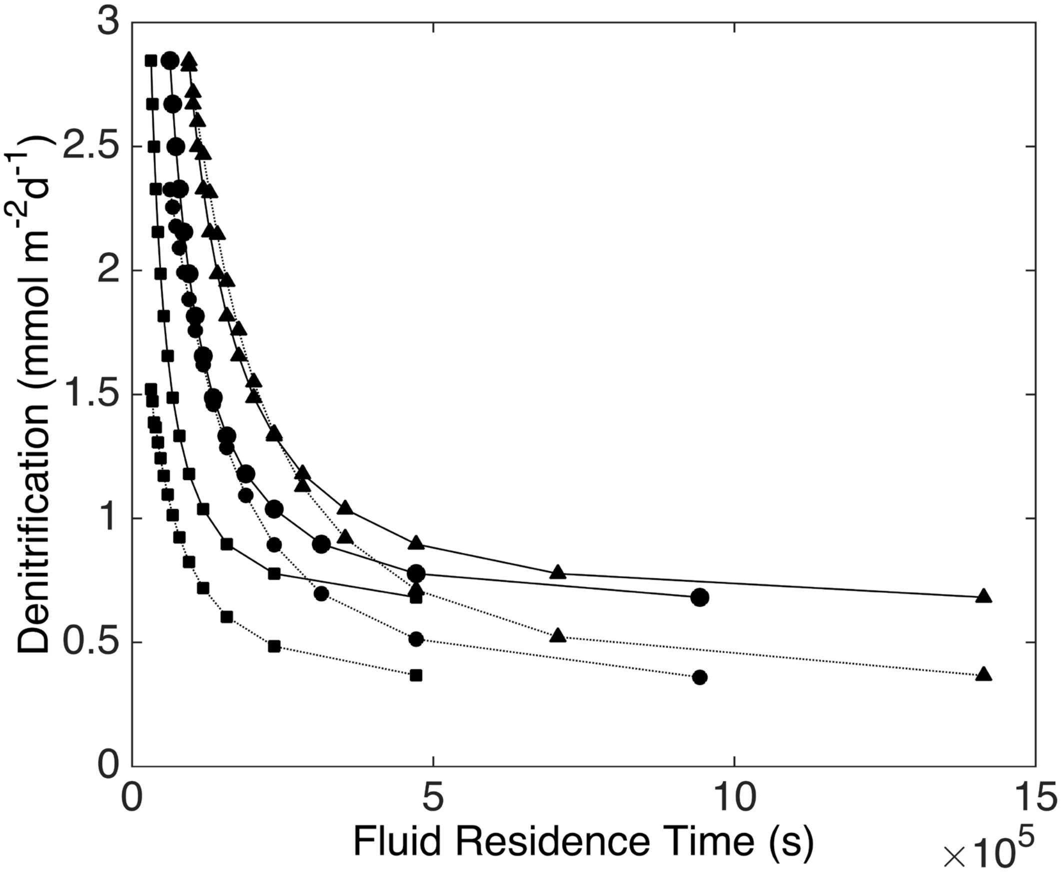
Denitrification (mmol m-2d-1)
Fluid Residence Time (s)
×10^5
0
0.5
1
1.5
2
2.5
3
0
5
10
15

Figure 5